From ADA309667 Downloaded from Digitized 02/25/2015
contrails.iit.edu

DAMPING CAPACITY OF ALUMINUM 6061-INDIUM ALLOYS.

C.R. Wong, D.C. Van Aken*, and O. Diehm*

David Taylor Research Center
Physical Metallurgy Branch
Code 2812
Annapolis, MD 21402-5067

*Dept. Materials Science and Engineering
University of Michigan
Ann Arbor, MI 48109-2136

ABSTRACT

Type 6061 aluminum alloys containing between 0 and 5.2 volume percent indium and pure indium samples were fabricated. Each sample was characterized by metallographic and analytical electron microscopy and the damping capacity and storage modulus was measured. The model proposed by L.G. Nielsen was used to calculate the damping capacity and storage modulus of the alloys using the damping capacity and storage modulus of the constituents. The damping capacity of the Al-6061-In-T6 alloys were higher than the Al-6061-T6 alloy and increased with increasing indium content. The Nielsen model gave a good first approximation of the damping capacity and storage modulus of the alloys.

Confirmed public via DTIC Online 02/25/2015

From ADA309667 Downloaded from Digitized 02/25/2015
contrails.iit.edu

DAMPING CAPACITY OF ALUMINUM 6061-INDIUM ALLOYS.

C.R. Wong, D.C. Van Aken*, and O. Diehm*
David Taylor Research Center
Physical Metallurgy Branch
Code 2812
Annapolis, MD 21402-5067

*Dept. Materials Science and Engineering
University of Michigan
Ann Arbor, MI 48109-2136

ABSTRACT

Type 6061 aluminum alloys containing between 0 and 5.2 volume percent indium and pure indium samples were fabricated. Each sample was characterized by metallographic and analytical electron microscopy and the damping capacity and storage modulus was measured. The model proposed by L.G. Nielsen was used to calculate the damping capacity and storage modulus of the alloys using the damping capacity and storage modulus of the constituents. The damping capacity of the Al-6061-In-T6 alloys were higher than the Al-6061-T6 alloy and increased with increasing indium content. The Nielsen model gave a good first approximation of the damping capacity and storage modulus of the alloys.

INTRODUCTION

An important characteristic of a structural material is it's damping capacity. While metallic materials exhibit adequate stiffness for structural use, the damping capacity may be quite low, having a typical loss factor on the order of 10^{-4}. In contrast, polymeric materials will exhibit very high damping, with loss factors on the order of one, but rather low stiffness. Their stiffness can be increased with the use of fillers and fibers but the resultant resin matrix composites exhibit lower damping properties, with loss factors on the order of 10^{-2}. Attempts made to improve the damping response of the resin matrix composite by adding rubber did not result in significant improvements [1]. It was shown that synergistic effects from interactions between the rubber and the resin were responsible for the lower than expected damping behavior.

In the case of metal matrix composites, work by Ray, Kinra, Rawal and Misra has shown that the damping of aluminum alloy 6061 is increased by the addition of graphite fibers [2]. However, the increase in damping was low considering the high volume fraction (0.34) of graphite. Recent work by Diehm, Wong and Van Aken has shown that the addition of a viscoelastic inclusion (indium) to pure aluminum will produce high damping materials [3], but it was uncertain whether the principal damping resulted from the matrix or the inclusion since both have high damping capacities.

In the present paper the addition of indium to an age-hardening alloy, such as 6061 aluminum, was examined in order to discriminate between inclusion and matrix damping. The dynamic properties of pure (99.99%) indium and 6061-T6 aluminum alloy were determined. The dynamic properties of the composite were calculated by using the values of the monolithic material in the composite model proposed by L.G. Nielsen [4,5] and directly compared with the experimental results.

Confirmed public via DTIC Online 02/25/2015

From ADA309667 Downloaded from Digitized 02/25/2015
contrails.iit.edu

NIELSEN MODEL

The model developed by Nielsen [4] predicts the complex modulus of isotropic two phase materials with arbitrary phase geometry. It is based on a continuum mechanics composite sphere assemblage model but is semi-empirical. The model assumes that the alloy is isotropic, strained only in the elastic range, and is phase symmetric, that is both the matrix and second phase geometries are identical at equal respective volume concentrations. Equations 1-4 below, from Nielsen's model [5], calculate Young's modulus of the alloy, E_y, using the Young's moduli of the matrix, E_y^s, and second phase, E_y^i, and the volume concentration, c. The volume concentration $= \frac{V^i}{(V^s + V^i)}$ where V^i and V^s are the volumes of the second phase and matrix respectively.

$$E_y = eE_y^s \qquad \text{eq.1}$$

where e is the relative Young's modulus of the alloy.

$$e = \frac{n + \gamma + \gamma c(n - 1)}{n + \gamma - c(n - 1)} \qquad \text{eq.2}$$

where n is the relative stiffness and γ is the shape function.

$$n = \frac{E_y^i}{E_y^s} \qquad \text{eq.3}$$

$$\gamma = \frac{1}{2}\left\{ \rho[1 - c(1 - n)] + \sqrt{\rho^2[1 - c(1 - n)]^2 + 4n(1 - \rho)} \right\} \qquad \text{eq.4}$$

and ρ is the shape factor which is dependent on the morphology of the composite.

The complex modulus of the matrix, E^s, and second phase, E^i, is defined as follows.

$$E^s = a^s + ib^s \quad \text{and} \quad E^i = a^i + ib^i \qquad \text{eq.5}$$

where a and b are the storage and loss modulus respectively and the superscripts s and i refer to the matrix and second phase respectively. The conversion from Young's modulus equations to complex modulus equations is accomplished with the use of the correspondence principle. The complex moduli from equation 5 are substituted for the Young's moduli in equations 1 and 3 and the real and imaginary parts are separated. Starting with equation 3 we have

$$n = \frac{E^i}{E^s} = \frac{a^i + ib^i}{a^s + ib^s} = \frac{(a^i + ib^i)(a^s - ib^s)}{(a^s + ib^s)(a^s - ib^s)} = \frac{a^ia^s + b^ib^s}{(a^s)^2 + (b^s)^2} + \frac{i(a^sb^i - a^ib^s)}{(a^s)^2 + (b^s)^2}$$

$$\text{Let } n = A + Bi \quad \text{where } A = \frac{a^ia^s + b^ib^s}{(a^s)^2 + (b^s)^2} \quad B = \frac{a^sb^i - a^ib^s}{(a^s)^2 + (b^s)^2} \qquad \text{eq.6}$$

Now recalling equation 4

$$\gamma = \frac{1}{2}\left\{ \rho[1 - c(1 - n)] + \sqrt{\rho^2[1 - c(1 - n)]^2 + 4n(1 - \rho)} \right\}$$

Confirmed public via DTIC Online 02/25/2015

From ADA309667 Downloaded from Digitized 02/25/2015
contrails.iit.edu

Upon substituting equation 6 the first part of equation 4 becomes

$$\rho[1 - c(1 - n)] = \rho - \rho c + \rho cn = \rho - \rho c + \rho cA + \rho cBi \qquad \text{eq.7}$$

The second part of equation 4 is $\sqrt{\rho^2[1 - c(1 - n)]^2+4n(1 - \rho)}$

$$\begin{aligned}[1 - c(1 - n)]^2 &= 1 - 2c(1 - n) + c^2(1 - n)^2 \\ &= 1 - 2c + 22n + c^2 - 2c^2n + c^2n^2 \\ &= 1 - 2c + c^2 + (2c - 2c^2)n + c^2n^2\end{aligned}$$

since $n^2 = (A + iB)(A + iB) = A^2 - B^2 + 2ABi$

$$\begin{aligned}\text{then } [1 - c(1 - n)]^2 &= (1 - 2c + c^2) + (2c - 2c^2)A + c^2(A^2 - B^2) \\ &\quad + i[(2c - 2c^2)B + 2c^2AB]\end{aligned}$$

$$\begin{aligned}\text{therfore } &\sqrt{\rho^2[1 - c(1 - n)]^2+4n(1 - \rho)} \\ &= \left\{\rho^2[1 - 2c + c^2 + (2c - 2c^2)A + c^2(A^2 - B^2)]\right. \\ &\quad \left. + i\rho^2[(2c - 2c^2)B + 2c^2AB] + 4A(1 - \rho) + i4B(1 - \rho)\right\}^{\frac{1}{2}} \\ &= \left\{\rho^2[1 - 2c + c^2 + 2c(1 - c)A + c^2(A^2 - B^2)]\right. \\ &\quad \left. + 4A(1 - \rho) + i[\rho^2 2c(1 - c)B + 2c^2AB\rho^2 + 4B(1 - \rho)]\right\}^{\frac{1}{2}}\end{aligned}$$

Let $\sqrt{\rho^2[1 - c(1 - n)]^2+4n(1 - \rho)} = [\alpha + i\beta]^{\frac{1}{2}}$ eq.8

where $\alpha = \rho^2[(c - 1)^2 - 2c(c - 1)A + c^2(A^2 - B^2)] + 4A(1 - \rho)$ eq.9

and $\beta = \rho^2 2c(1 - c)B + 2c^2AB\rho^2 + 4B(1 - \rho)$ eq.10

In order to find the square root we change coordinates.

$$r = (\alpha^2 + \beta^2)^{\frac{1}{2}} \qquad \text{eq.11}$$

$$\theta = \arctan\left[\sqrt{\frac{\beta}{\alpha}}\right] \qquad \text{eq.12}$$

substituting equations 11 and 12 into equation 8 we have

$$\sqrt{\rho^2[1 - c(1 - n)]^2+4n(1 - \rho)} = r^{1/2}[\cos(\theta/2)+i\sin(\theta/2)] = r^{1/2}e^{i\theta/2} \qquad \text{eq.13}$$

Combining equations 7 and 13 gives the complex shape function, γ^*.

$$\gamma^* = \frac{1}{2}\left\{\rho[1 - c(1 - A)] + \rho cBi + r^{1/2}e^{i\theta/2}\right\} \qquad \text{eq.14}$$

Confirmed public via DTIC Online 02/25/2015

From ADA309667 Downloaded from Digitized 02/25/2015
contrails.iit.edu

Substituting the complex values of γ from equation 14 and the complex values of n from equation 6 into equation 2 gives the complex relative modulus, e^*.

$$e^* = \frac{n + \gamma^* + \gamma^* c(n-1)}{n + \gamma^* - c(n-1)} = \frac{n + \gamma^* + cn\gamma^* - \gamma^* c}{n + \gamma^* - cn + c}$$

$$= \frac{A + Re(\gamma^*) - cRe(\gamma^*) + c[ARe(\gamma^*) - BIm(\gamma^*)]}{(A + Re(\gamma^*) - cA + c) + i(B + Im(\gamma^*) - cB)}$$

$$+ \frac{i\{B + Im(\gamma^*) - cIm(\gamma^*) + c[AIm(\gamma^*) + BRe(\gamma^*)]\}}{(A + Re(\gamma^*) - cA + c) + i(B + Im(\gamma^*) - cB)} \qquad \text{eq.15}$$

Let $\xi = A + Re(\gamma^*) - cRe(\gamma^*) + c[ARe(\gamma^*) - BIm(\gamma^*)]$ eq.16

and $\eta = B + Im(\gamma^*) - cIm(\gamma^*) + c[AIm(\gamma^*) + BRe(\gamma^*)]$ eq.17

and substitute into equation 15.

$$e^* = \frac{\xi + \eta i}{(A + Re(\gamma^*) - cA + c) + i(B + Im(\gamma^*) - cB)}$$

$$= \frac{(\xi + i\eta)[(A + Re(\gamma^*) - cA + c) - i(B + Im(\gamma^*) - cB)]}{(A + Re(\gamma^*) - cA + c)^2 + (B + Im(\gamma^*) - cB)^2}$$

$$= \frac{\xi(A + Re(\gamma^*) - cA + c) + \eta(B + Im(\gamma^*) - cB)}{(A + Re(\gamma^*) - cA - c)^2 + (B + Im(\gamma^*) - cB)^2}$$

$$+ \frac{i\eta(A + Re(\gamma^*) - cA + c) - \xi(B + Im(\gamma^*) - cB)}{(A + Re(\gamma^*) - cA - c)^2 + (B + Im(\gamma^*) - cB)^2} \qquad \text{eq.18}$$

Finally the complex modulus of the alloy is found by combining equations 1, 5 and 18.

$$E^i = e^* E^s = Re(e^*)a^s - Im(e^*) + i[Im(e^*) + Re(e^*)b^s]$$

$$= \frac{a^s[\xi(A + Re(\gamma^*) - cA + c) + \eta(B + Im(\gamma^*) - cB)]}{(A + Re(\gamma^*) - cA - c)^2 + (B + Im(\gamma^*) - cB)^2}$$

$$- \frac{b^s[\eta(A + Re(\gamma^*) - cA + c) - \xi(B + Im(\gamma^*) - cB)]}{(A + Re(\gamma^*) - cA - c)^2 + (B + Im(\gamma^*) - cB)^2}$$

$$+ i\left\{\frac{a^s[\eta(A + Re(\gamma^*) - cA + c) - \xi(B + Im(\gamma^*) - cB)]}{(A + Re(\gamma^*) - cA - c)^2 + (B + Im(\gamma^*) - cB)^2}\right.$$

$$\left. + \frac{b^s[\xi(A + Re(\gamma^*) - cA + c) + \eta(B + Im(\gamma^*) - cB)]}{(A + Re(\gamma^*) - cA - c)^2 + (B + Im(\gamma^*) - cB)^2}\right\} \qquad \text{eq.19}$$

Where the real of equation 19 is the storage modulus of the composite and the imaginary part of equation 19 is the loss modulus.

Confirmed public via DTIC Online 02/25/2015

From ADA309667 Downloaded from Digitized 02/25/2015
contrails.iit.edu

EXPERIMENTAL PROCEDURE

Aluminum 6061 alloys with additions of 0 to 12 weight percent indium were prepared by plasma arc-melting. The starting alloys were pure indium (99.99%) and 6061 alloy. The chemical composition of the alloys were determined by wet-chemistry. The volume fraction of indium was calculated using the weight fraction and density of each alloy by assuming complete immiscibility between aluminum and indium. The arc-melted ingot was then reduced 60 to 80% in thickness, by repeatedly cold-working 20 to 30% and annealing, to produce a flat sample with a nominal thickness of 1.5 mm. The alloys were given a T6 temper consisting of solution treatment at 532 °C (990 °F) and aging 193 oC (380 °F) for 7 hours. Samples of pure indium were likewise plasma arc-melted and rolled.

Each sample was characterized by metallographic and analytical electron microscopy. Electron microscopy studies were performed at the University of Michigan Electron Microbeam Analysis Laboratory. Thin foils for transmission electron microscopy were prepared by twin jet electropolishing in a solution of 20% nitric acid (by volume) and methanol.

The damping capacity and modulus of the samples were measured with a Polymer Laboratories Dynamic Mechanical Thermal Analyzer (DMTA) located at the Naval Research Laboratory. The DMTA uses a fixed-guided cantilever arrangement where the left clamp holds the sample to a stationary frame while the right clamp attaches the sample to the drive shaft. A small sinusoidal mechanical stress is applied to a cantilevered sample and the resulting sinusoidal strain is transduced. Comparison of the amplitude of the stress, σ, and strain, ϵ, signals yields the storage modulus, a, and the phase lag of strain behind the stress gives the phase angle, δ. The complex modulus, E, and loss modulus b are calculated using the following equation:

$$a(1 + i\tan\delta) = E = a + ib \qquad \text{eq.20}$$

where tan δ is the loss factor. The frequency of the vibrations was cycled between .1, 1 and 10 Hz while the temperature was increased one degree C per minute from 20 °C (68 °F) to 100 °C (212 °F). Each sample was measured at least twice to check the consistency of the measurements.

RESULTS

The measured chemical composition and the calculated volume fraction of indium are presented in table 1. The volume percent varied from 0 to 5.2. The microstructures of the indium containing alloys are shown in Fig. 1. A uniform dispersion of indium particles was found in all the samples with the individual areas of indium increasing in size and number with the increase in volume percent. The micrographs show the indium phase to be roughly spherical. Examination of the age-hardened matrix using transmission electron microscopy revealed that the age-hardening process was affected by the addition of indium. A typical 6061 T6 microstructure consists of a uniform distribution of Guinier-Preston zones (GPZ) and β' (rod shaped Mg_2Si) precipitates in the aluminum matrix as shown in Fig. 2a. The diffraction conditions are optimized in Figs. 2a and 2b to show the β'

Confirmed public via DTIC Online 02/25/2015

From ADA309667 Downloaded from Digitized 02/25/2015
contrails.iit.edu

precipitates. The aged microstructures of the alloys, containing 1.4, 1.7, and 5.2 volume percent indium are shown in Figs. 2b to 2d. It is apparent that the aging kinetics have been affected by the additions of indium. The general trend is that the precipitation of β' is inhibited and the volume fraction of second phase is reduced. Only the GPZ's are observed in the 1.7 and 5.2% alloys.

The results of the DMTA testing are shown as plots of loss modulus, (tan δ), versus the storage modulus on logarithmic axis in order to eliminate temperature and frequency measurement error from the data. As the temperature was increased from 20 °C to 100 °C the loss factor increased as the storage modulus decreased. The measurements of pure indium and the 6061 T6 alloy are shown in Fig. 3. For the temperature range tested, the storage modulus of the 6061 T6 alloy did not vary significantly from 71 GPa while the storage modulus of the indium varied from 2 GPa at room temperature to 0.9 GPa at 100 °C. The loss factor of the 6061 T6 alloy was approximately 0.002 which is typical of precipitation hardened aluminum alloys. In contrast the pure indium alloy exhibited high damping with the loss factor ranging from 0.06 to 0.2 at 100 °C. It was generally observed that the storage modulus decreased and the loss factor increased with increasing addition of indium as shown in Fig. 4. The storage modulus of the sample containing 5.2 volume percent indium exhibited a more dramatic change than alloys containing less than 3.2 volume percent indium, as illustrated in Fig. 4. The loss factor of the 5.2 volume percent indium alloy at room temperature was measured to be 0.01. This was likely due to increased continuity of the indium phase.

The storage modulus and loss factor were calculated with the Nielsen model using the data from the monolithic material in equations 19 and 20 and a shape factor of one. A shape factor of one describes round second phase areas completely surrounded by the matrix. The results of these calculations are presented in Fig. 5. The calculated and measured values of the 0 volume percent indium alloy are constrained to be equal. Comparing the calculated values to the measured values as in Fig. 6 and 7 it is obvious that although the calculated values show the same trends as the measured values, they consistently overestimate both the measured storage modulus and the loss factor of the alloys. For the alloys containing less than 3.2 volume percent the storage modulus is only overestimated by 2% and the loss factor is overestimated by 30%. However, in the case of the 5.2 volume percent indium alloy the storage modulus was overestimated by more than 100% while the loss factor was overestimated by 60%. These results may indicate a synergistic effect such as the partitioning of alloying elements present in the 6061 material to the indium.

DISCUSSION

High damping aluminum alloys may be obtained by the addition of a viscoelastic inclusion. In the present case a volume fraction of at least 0.05 is required to produce an alloy with a loss factor greater than 0.01. However, there is a significant loss of stiffness associated with the addition of the indium and there appears to be a synergistic effect between the matrix and the inclusion. The aged 6061-T6 microstructure shows a decreasing precipitate density with increasing indium content and the measured loss factors are much less than the

Confirmed public via DTIC Online 02/25/2015

From ADA309667 Downloaded from Digitized 02/25/2015
contrails.iit.edu

calculated values based on the damping capacities of the monolithic samples. It is tempting to speculate that these observations are related. Indeed, the solubility of magnesium in indium is greater than 30 atomic percent at the T6 aging temperature used in this experiment [6]. Thus the low volume fraction of precipitates may be related to the partitioning of magnesium to the indium inclusions. Furthermore, the indium-magnesium inclusions may have a lower damping capacity than the pure indium. If indeed the damping of the indium inclusion is a strain dependent mechanism, such as dislocation motion, the addition of solute atoms will result in a lower loss factor for a comparable cyclic strain.

The Nielsen model failed to predict the dynamic properties of indium containing 6061-T6 alloys, but did provide a good first approximation. Future modeling of this system will use the dynamic properties measured from monolithic indium-magnesium alloys to compensate for the synergistic effects encountered and the shape factor will be varied in an attempt to compensate for non-spherical inclusions.

CONCLUSIONS

Additions of indium, a viscoelastic second phase particle, to 6061-T6 aluminum, a stiff matrix, have resulted in an increased damping capacity while still maintaining most of the stiffness of the matrix. The measured and calculated values agree that damping capacity increases and the storage modulus decreases with increasing indium content. The Nielsen model is a good first approximation for both the prediction of the maximum damping capacity and stiffness of a particular alloy system and the tailoring of alloys to obtain the damping capacity and stiffness required by a given application.

ACKNOWLEDGMENTS

The assistance of Dr. M.A. Imam and Mr. K. Robinson of the Naval Research Laboratory with the operation of the DMTA and Mr. J. Newton of the University of Missouri Dept. of Physics with the complex algebra is greatly appreciated.

Confirmed public via DTIC Online 02/25/2015

From ADA309667 Downloaded from Digitized 02/25/2015
contrails.iit.edu

REFERENCES

1. G. Rohrauer, S.V. Hoa and D. Feldman, 5th Inter. Conf. Composite Materials, Eds. Harrigan, Strife, and Dhingra, The Minerals, Metals & Materials Society, (1986) p. 1683.

2. A,K. Ray, V.K. Kinra, S.P. Rawal, and M.S. Misra, Role of Interfaces on Material Damping, Eds. B.B. Rath and M.S. Misra, ASM International, (1985) p. 95.

3. O. Diehm, C.R. Wong, and D.C. Van Aken, this conference proceedings, JDA1.

4. Nielsen, L.G. "Elastic Properties of Two-phase Materials", Materials Science and Engineering, Vol. 52 (1982) p. 39.

5. Nielsen, L.G. "Elasticity and Damping of Porous Materials and Impregnated Materials", J. Amer. Ceramic Soc., Vol. 67 No. 2, (1984) p. 93.

6. A.A. Nayeb-Hashemi and J.B. Clark, Bull. Alloy Phase Diagrams, Vol. 6, (1985) p. 2

Table 1. Chemical Compositions of 6061-T6 Aluminum Alloys

Calculated Volume Percent	Measured Weight Percent						
Indium	Indium	Magnesium	Chromium	Silicon	Copper	Iron	Aluminum
0.00	0.00	0.77	0.048	0.71	0.26	0.23	98 97
0.78	2.08	0.74	0.047	0.83	0.27	0.25	95.78
1.43	3.77	0.70	0.046	0.76	0.26	0.24	94.22
1.67	4.37	0.67	0.045	0.73	0.25	0.22	93.72
2.16	5.63	0.70	0.044	0.75	0.26	0.22	92.40
2.66	6.87	0.73	0.045	0.71	0.25	0.21	91.19
3.20	8.20	0.73	0.041	0.70	0.28	0.22	89.83
5.16	12.80	0.70	0.042	0.64	0.23	0.20	85.39

Confirmed public via DTIC Online 02/25/2015

From ADA309667 Downloaded from Digitized 02/25/2015
contrails.iit.edu

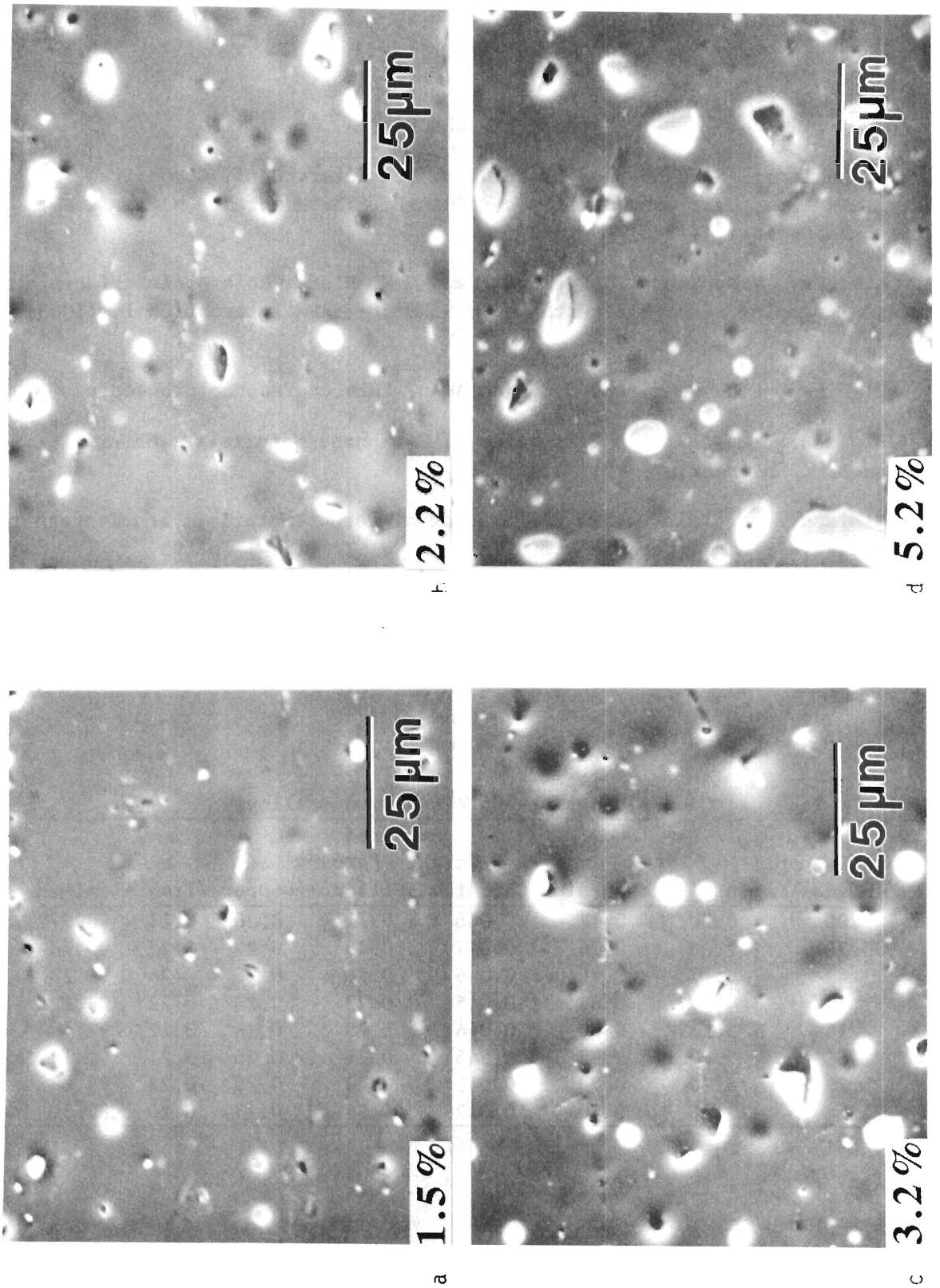

FIG. 1 MICROSTRUCTURES OF 6061-T6 ALUMINUM WITH 1.4 - 5.2 VOLUME PERCENT INDIUM

Confirmed public via DTIC Online 02/25/2015

FIG. 2 PRECIPITATES IN 6061-T6 ALUMINUM WITH 0 - 5.2 VOLUME PERCENT INDIUM

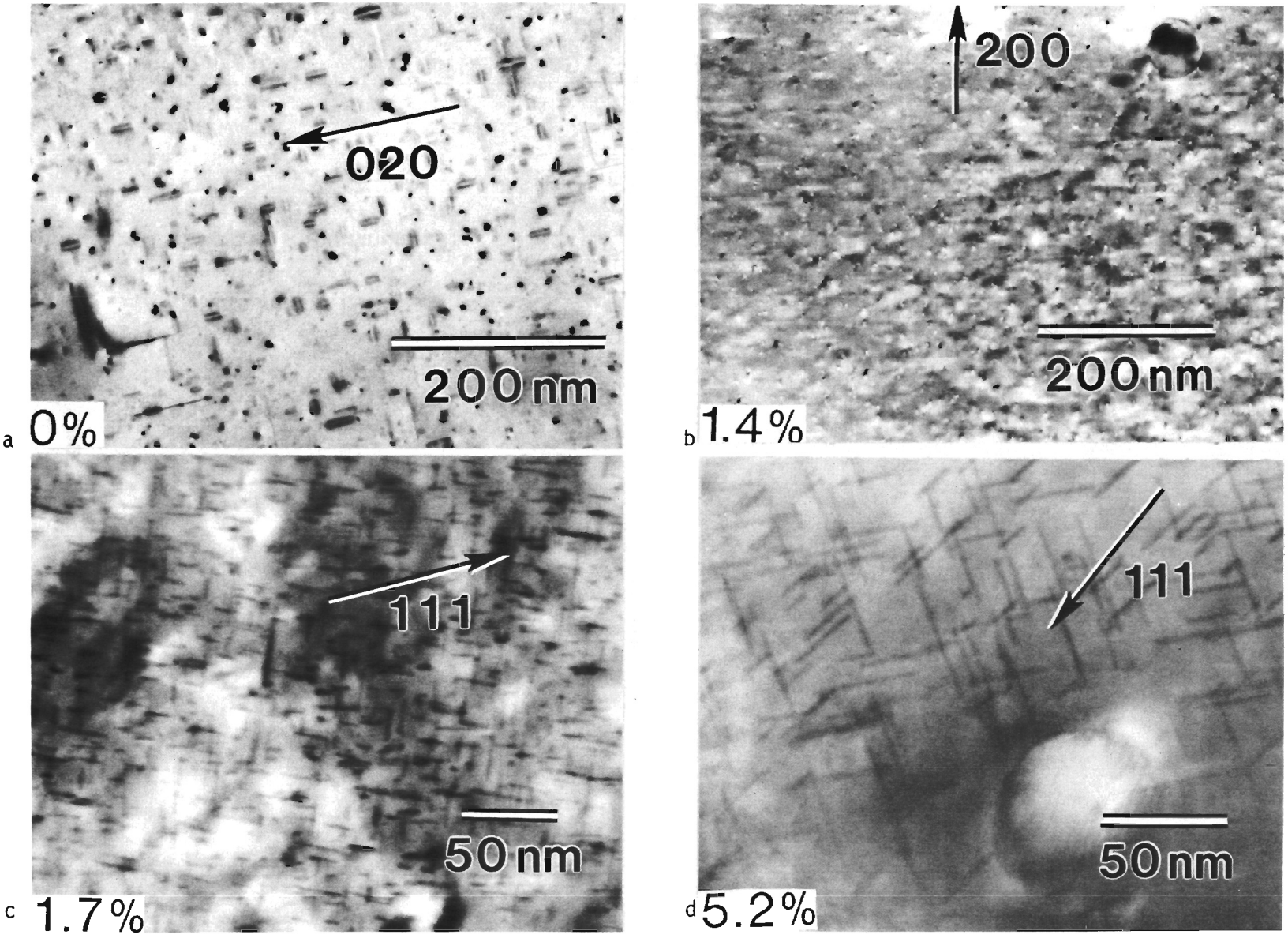

From ADA309667
Downloaded from contrails.iit.edu
Digitized 02/25/2015
Confirmed public via DTIC Online 02/25/2015

From ADA309667 Downloaded from Digitized 02/25/2015
contrails.iit.edu

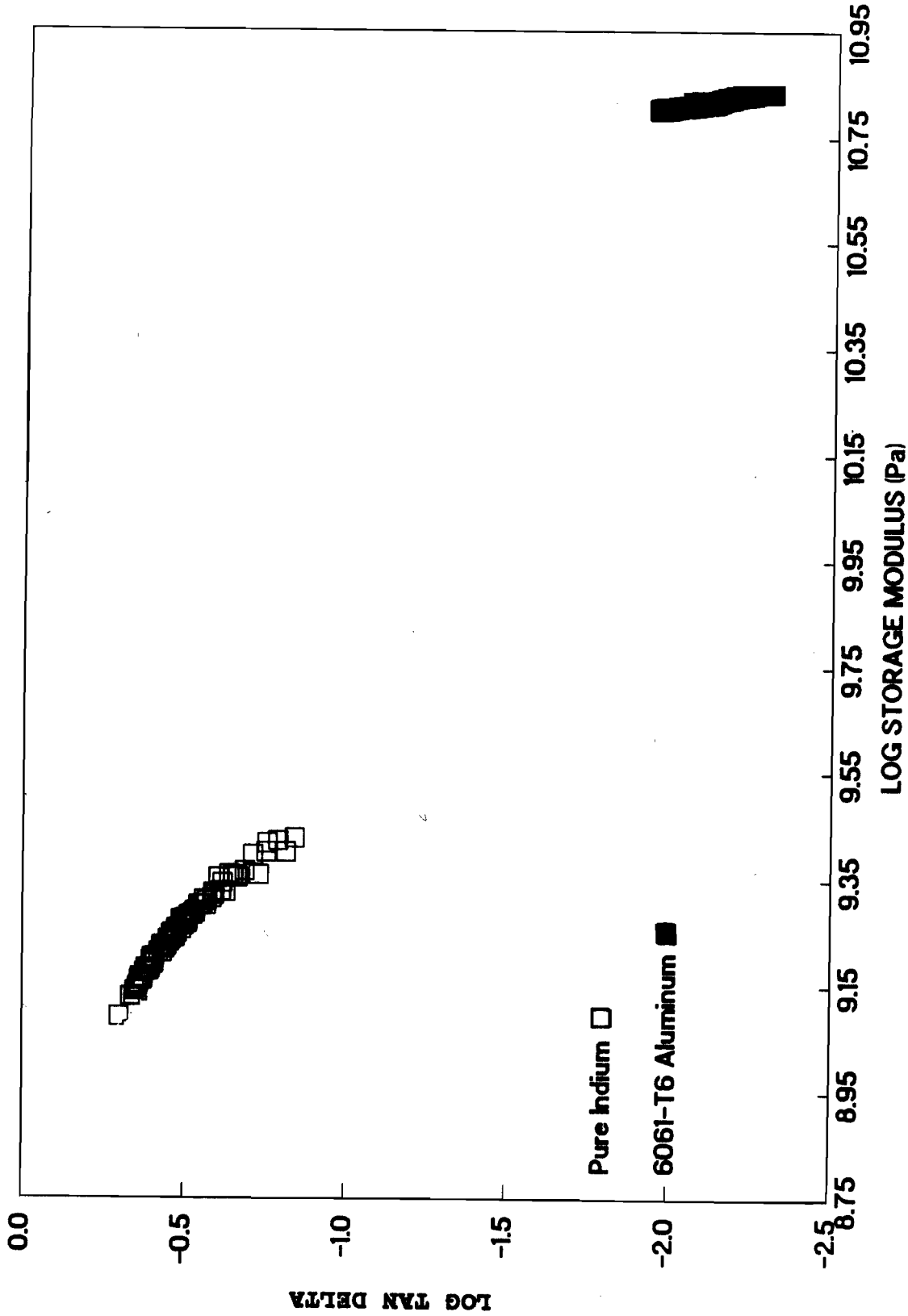

Fig. 3. Measured Values of the Loss Factor and Storage Modulus of the Monolithic Materials.

JDB12

Confirmed public via DTIC Online 02/25/2015

From ADA309667 Downloaded from Digitized 02/25/2015
contrails.iit.edu

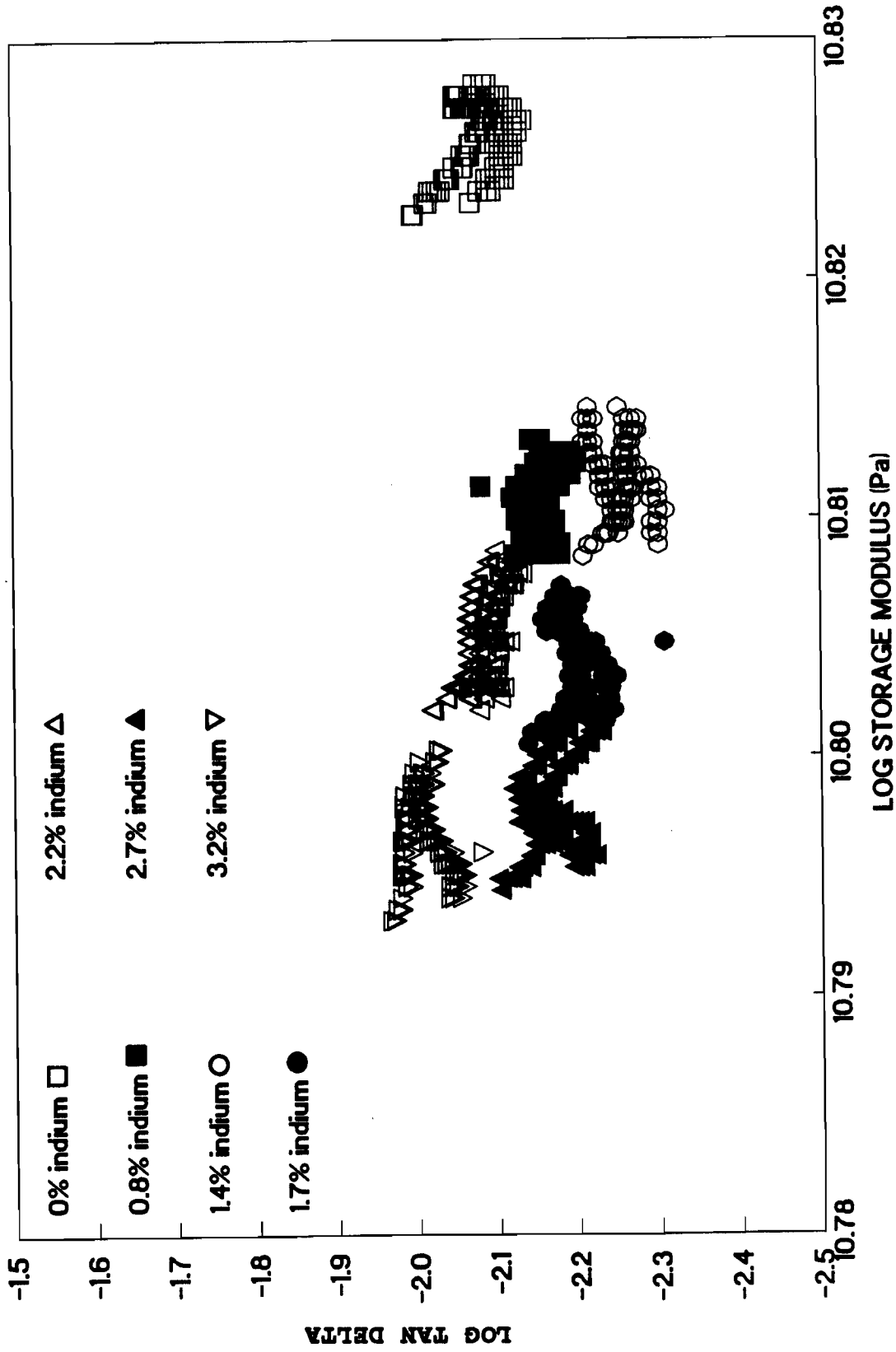

Fig. 4. Measured Values of the Loss Factor and Storage Modulus of 6061 Aluminum with 0 to 3.2 Volume Percent Indium.

JDB13

Confirmed public via DTIC Online 02/25/2015

From ADA309667 Downloaded from Digitized 02/25/2015
contrails.iit.edu

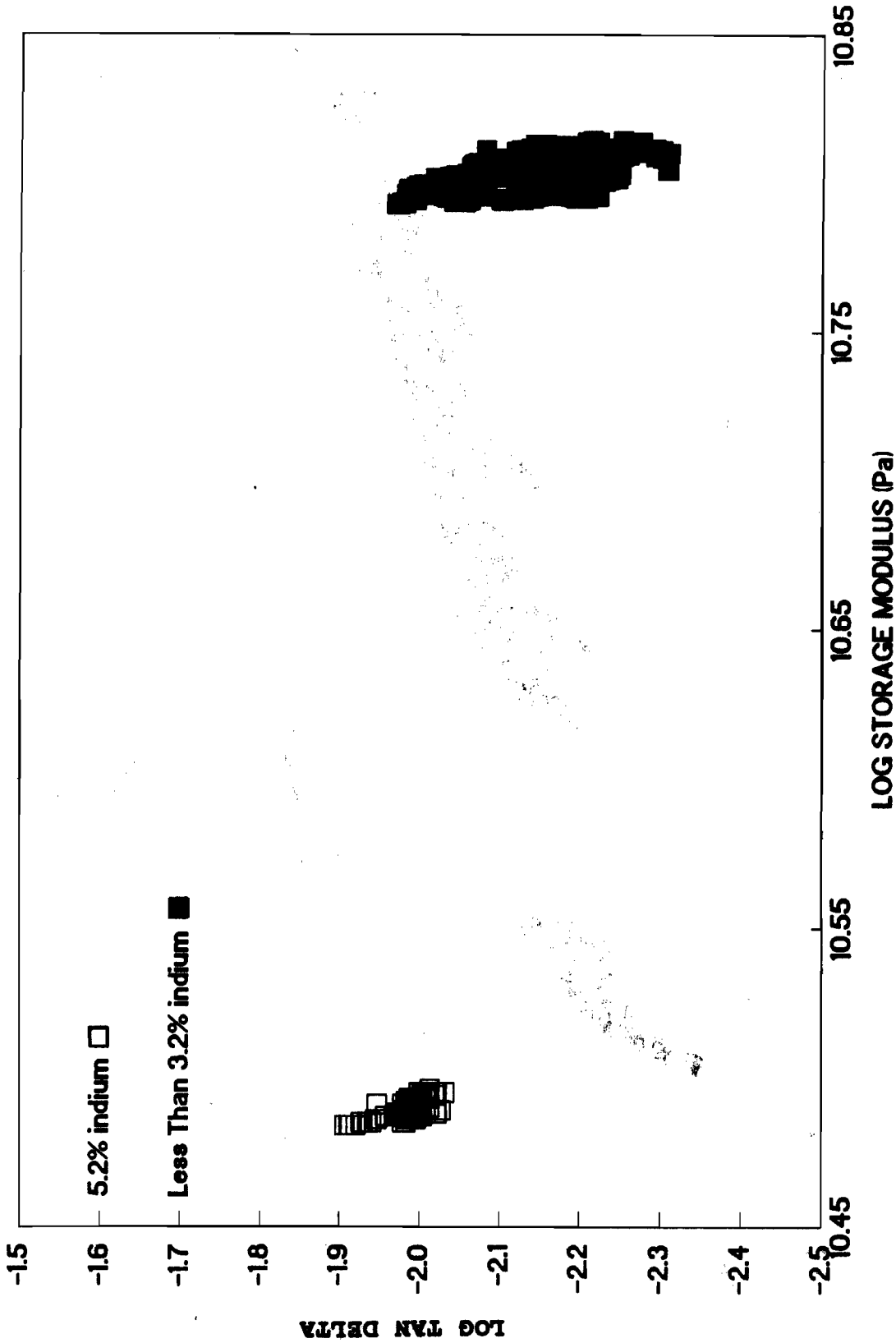

Fig. 5. Measured Values of the Loss Factor and Storage Modulus of 6061 Aluminum with 0 to 5.2 Volume Percent Indium.

JDB14

Confirmed public via DTIC Online 02/25/2015

From ADA309667 Downloaded from Digitized 02/25/2015
contrails.iit.edu

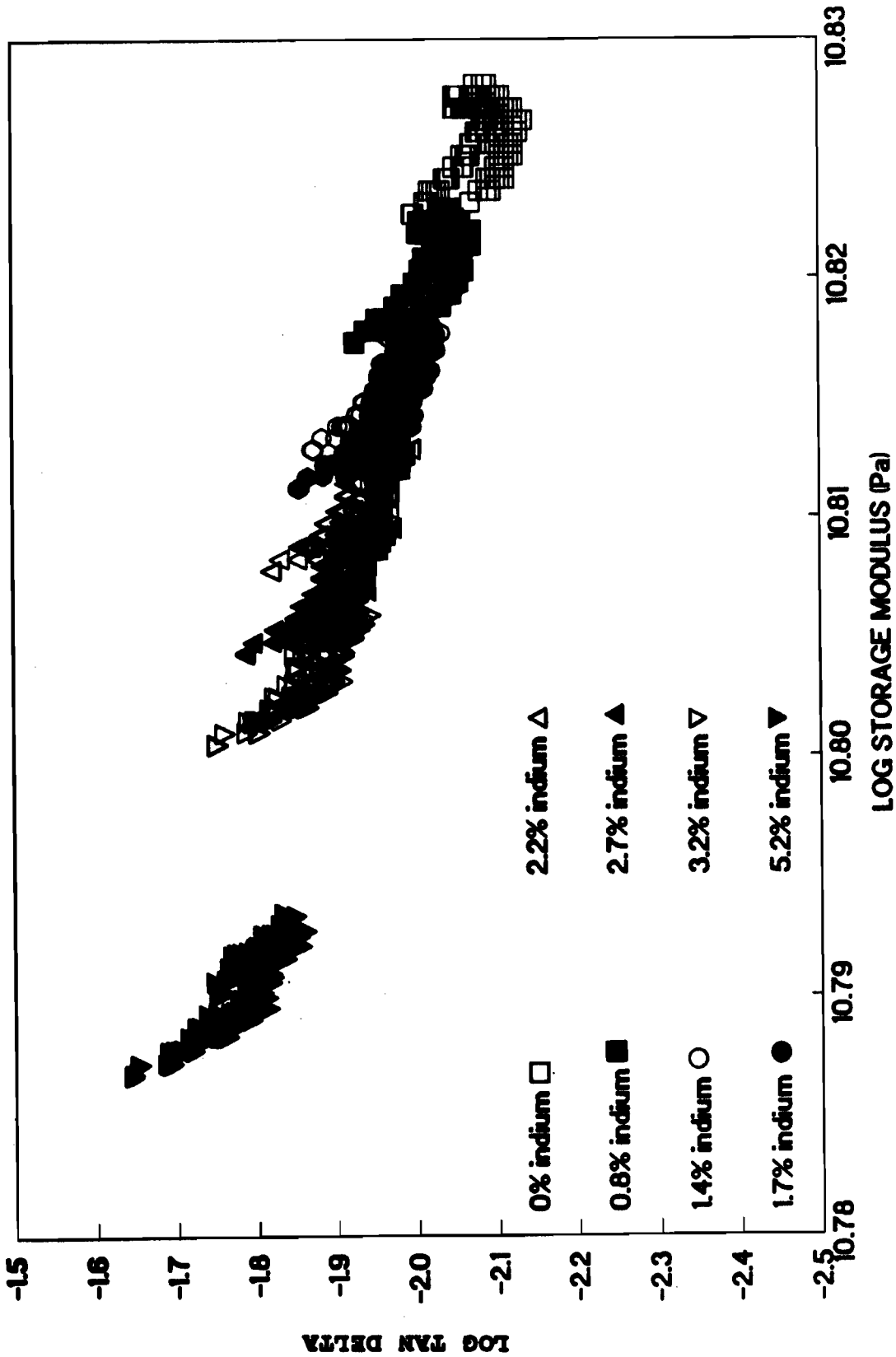

Fig. 6. Calculated Values of the Loss Factor and Storage Modulus of 6061 Aluminum with 0 to 3.2 Volume Percent Indium.

JDB15

Confirmed public via DTIC Online 02/25/2015

From ADA309667 Downloaded from Digitized 02/25/2015
contrails.iit.edu

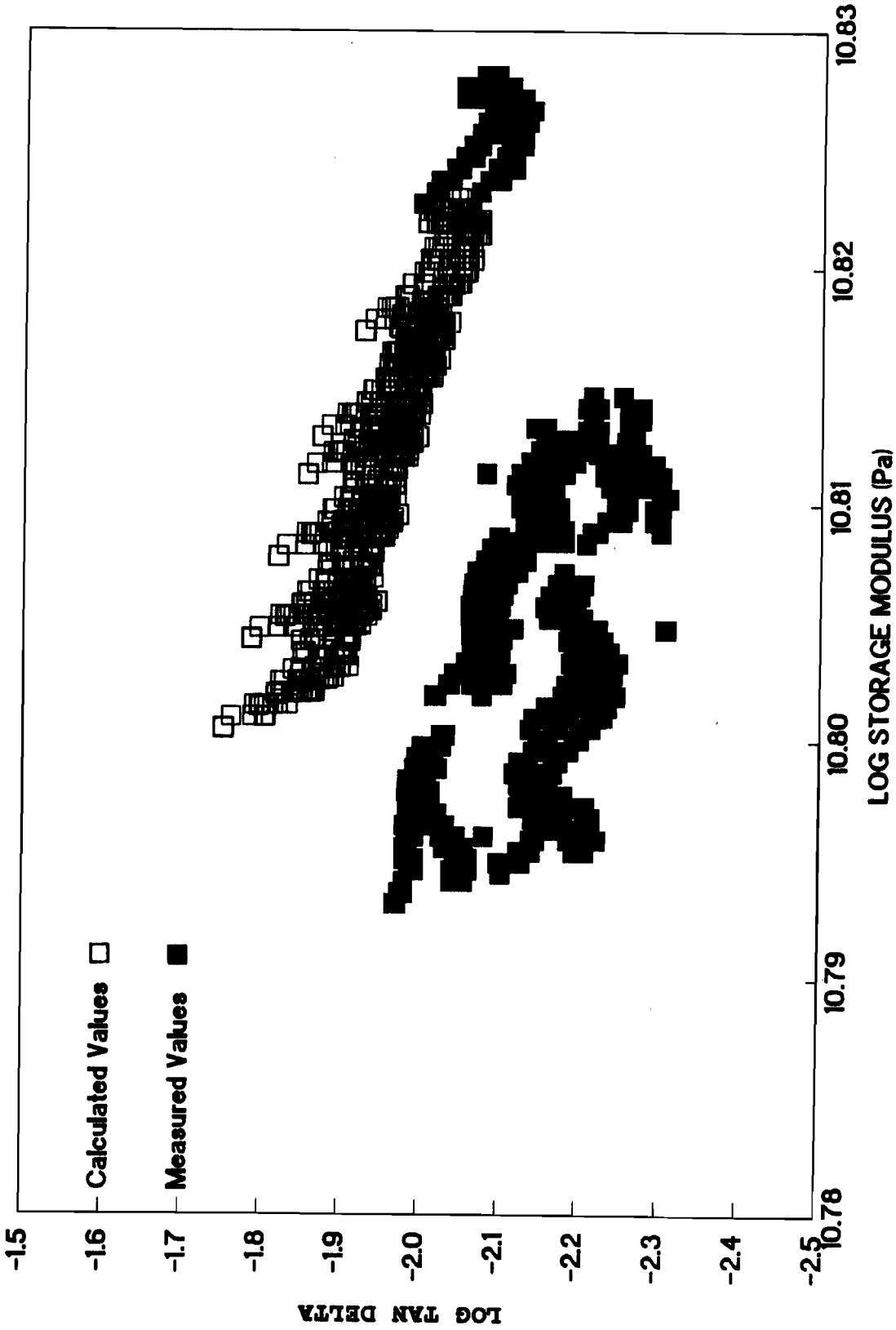

Fig. 7. Comparison of Measured and Calculated Values of the Loss Factor and Storage Modulus of 6061 Aluminum with 0 to 3.2 Volume Percent Indium.

JDB16

Confirmed public via DTIC Online 02/25/2015

From ADA309667 Downloaded from Digitized 02/25/2015
contrails.iit.edu

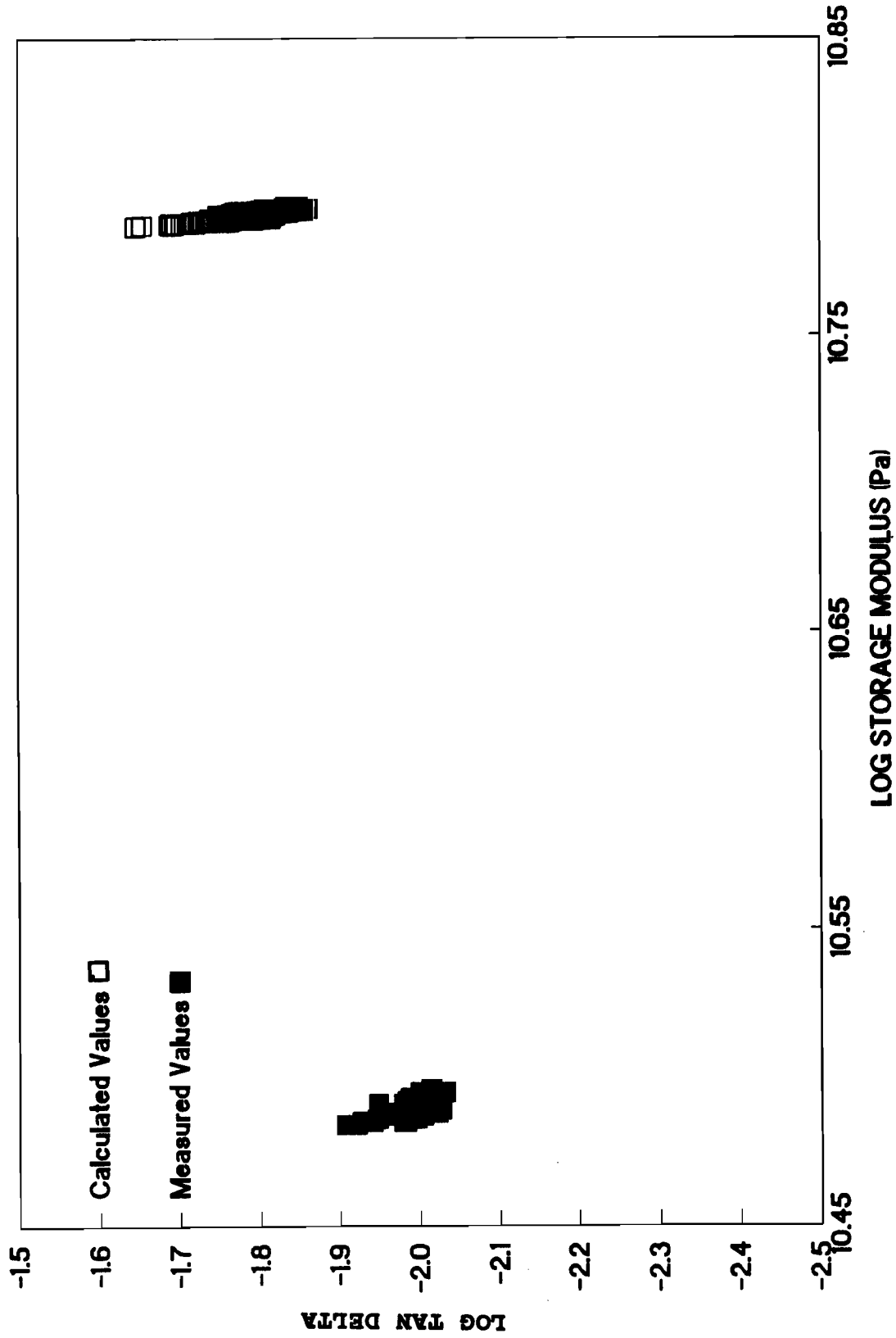

Fig. 8. Comparison of Measured and Calculated Values of the Loss Factor and Storage Modulus of 6061 Aluminum with 5.2 Volume Percent Indium.

JDB17

Confirmed public via DTIC Online 02/25/2015